NeuroImage: Clinical 34 (2022) 103021

Contents lists available at ScienceDirect

NeuroImage: Clinical

journal homepage: www.elsevier.com/locate/ynicl

Evaluating iron deposition in gray matter nuclei of patients with unilateral middle cerebral artery stenosis using quantitative susceptibility mapping

Huimin Mao [a,b,1], Weiqiang Dou [c,1], Kunjian Chen [a,b], Xinyu Wang [a,b], Xinyi Wang [a,*], Yu Guo [a,b], Chao Zhang [a]

[a] Department of Radiology, The First Affiliated Hospital of Shandong First Medical University & Shandong Provincial Qianfoshan Hospital, Jinan, Shandong Province 250014, China
[b] Shandong First Medical University, Jinan, Shandong Province 250000, China
[c] MR Research, GE Healthcare, Beijing 10076, China

ARTICLE INFO

Keywords:
Middle cerebral artery stenosis or occlusion
Cerebral ischemia
Quantitative susceptibility mapping
Iron deposition
Gray matter nuclei

ABSTRACT

Iron mediated oxidative stress is involved in the process of brain injury after long-term ischemia. While increased iron deposition in the affected brain regions was observed in animal models of ischemic stroke, potential changes in the brain iron content in clinical patients with cerebral ischemia remain unclear. Quantitative susceptibility mapping (QSM), a non-invasive magnetic resonance imaging technique, can be used to evaluate iron content in the gray matter (GM) nuclei reliably. In this study, we aimed to quantitatively evaluate iron content changes in GM nuclei of patients with long-term unilateral middle cerebral artery (MCA) stenosis/occlusion-related cerebral ischemia using QSM.

Forty-six unilateral MCA stenosis/occlusion patients and 38 age-, sex- and education-matched healthy controls underwent QSM. Clinical variables of history of hypertension, diabetes, hyperlipidemia, hyperhomocysteinemia, smoking, and drinking in all patients were evaluated. The iron-related susceptibility of GM nucleus subregions, including the bilateral caudate nucleus (CN), putamen (PU), globus pallidus (GP), thalamus, substantia nigra (SN), red nucleus, and dentate nucleus, was assessed. Susceptibility was compared between the bilateral GM nuclei in patients and controls. Receiver operating characteristic curve analysis was used to evaluate the efficacy of QSM susceptibility in distinguishing patients with unilateral MCA stenosis/occlusion from healthy controls. Multiple linear regression analysis was used to evaluate the relationship between ipsilateral susceptibility levels and clinical variables.

Except for the CN, the susceptibility in most bilateral GM nucleus subregions was comparable in healthy controls, whereas for patients with unilateral MCA stenosis/occlusion, the ipsilateral PU, GP, and SN exhibited significantly higher susceptibility than the contralateral side (all $P < 0.05$). Compared with controls, susceptibility of the ipsilateral PU, GP, and SN and of contralateral PU in patients were significantly increased (all $P < 0.05$). The area under the curve (AUC) was greater for the ipsilateral PU than for the GP and SN (AUC = 0.773, 0.662 and 0.681; all $P < 0.05$). Multiple linear regression analysis showed that the increased susceptibility of the ipsilateral PU was significantly associated with hypertension, of the ipsilateral GP associated with smoking, and of the ipsilateral SN associated with diabetes (all $P < 0.05$).

Our findings provide support for abnormal iron accumulation in the GM nuclei after chronic MCA stenosis/occlusion and its correlation with some cerebrovascular disease risk factors. Therefore, iron deposition in the GM nuclei, as measured by QSM, may be a potential biomarker for long-term cerebral ischemia.

* Corresponding author at: Department of Radiology, The First Affiliated Hospital of Shandong First Medical University (Shandong Provincial Qianfoshan Hospital), No.16766, Jingshi Rd, Jinan 250014, Shandong Province, China.
E-mail address: wxy_88@163.com (X. Wang).

[1] The first two authors contributed equally to this work.

https://doi.org/10.1016/j.nicl.2022.103021
Received 2 October 2021; Received in revised form 17 March 2022; Accepted 23 April 2022
Available online 26 April 2022

1. Introduction

Ischemic stroke is one of the main causes of adult disability and death.(Kuriakose and Xiao, 2020) Intracranial artery stenosis is the main cause of ischemic stroke, with the highest proportion being due to middle cerebral artery (MCA) stenosis or occlusion.(Ran et al., 2020) When unilateral MCA stenosis or occlusion occurs, it causes ischemia and hypoxia in brain tissues in the corresponding blood supply region, resulting in neuronal damage. A series of pathophysiological reactions, including oxidative stress induced by iron deposition, are involved in the process of brain injury after long-term ischemia and hypoxia (Sekerdag et al., 2018).

Iron is a double-edged sword in the dynamic balance of brain tissues: on the one hand, it is an essential element for the maintenance of normal brain function as it participates in several biological processes, including oxygen binding and transportation, electron transport, protein and DNA synthesis, neurotransmitter synthesis, and myelination (Connor et al., 2001) on the other hand, the brain is extremely vulnerable to iron-dependent oxidative stress. When the iron homeostasis is destroyed, excessive iron is deposited in the brain, triggering abnormal release of reactive oxygen species, oxidative stress, and cell death, which, in turn, cause organic or functional damage to brain tissues (Hubler et al., 2015; Apostolakis and Kypraiou, 2017). The occurrence and development of several neurological diseases have been reported to correlate closely with abnormal iron metabolism in the brain (Stankiewicz et al., 2007; Hayflick et al., 2018). Iron deposition in the affected brain region has been observed in animal models of ischemic stroke due to unilateral MCA occlusion (Tuo et al., 2017). Following severe ischemic-anoxic insults, four children showed hypointensity in the basal ganglia on T2-weighted imaging (T2WI), which may be related to iron deposition (Dietrich and Bradley, 1988). However, quantitative information regarding iron deposition cannot be provided only by observing changes in signal intensity on T2WI.

To address this issue, quantitative susceptibility mapping (QSM), a promising magnetic resonance imaging (MRI) technique for quantifying the spatial distribution of magnetic susceptibility in biological tissues, has been proposed (Vinayagamani et al., 2021). By reconstructing magnetic susceptibility sources from field perturbations, the iron levels in tissues can be measured using QSM (Vinayagamani et al., 2021). The susceptibility measured by QSM has been reported to be positively correlated with the average iron levels in the brain tissue, and QSM is currently the main method for the quantitative clinical measurement of iron content in living tissues (Langkammer et al., 2012; Haacke et al., 2015). Recently, QSM has identified excessive iron deposition in the brain, particularly in the gray matter (GM) nuclei, in various neurodegenerative diseases. Acosta-Cabronero et al (Acosta-Cabronero et al., 2013) utilized QSM to study the relationship between brain iron alterations and Alzheimer's disease (AD) and found that the iron content in the putamen (PU) of patients was significantly increased. Several studies have reported significantly elevated iron-related susceptibility in the substantia nigra (SN), as assessed using QSM, in patients with early Parkinson's disease (PD), and that the iron content was positively correlated with the PD severity score (Du et al., 2016; He et al., 2015). Domínguez et al. (Domínguez D et al., 2016) found that the QSM susceptibility of the caudate nucleus (CN), PU, and globus pallidus (GP) in patients with Huntington's disease (HD) was higher than that in healthy controls and that the susceptibility of the PU and CN in symptomatic patients with HD was positively correlated with disease severity. While promising quantitative iron results have been obtained in several neurodegenerative diseases, potential changes in the cerebral iron content in patients with cerebral ischemia have not been systematically explored so far.

Therefore, in this study, the main goal was to explore whether iron metabolism in the brain tissue was altered after long-term cerebral ischemia. Noninvasive QSM imaging was applied to evaluate changes in the iron content in the deep GM nuclei of the brain in patients with cerebral ischemia caused by long-term unilateral MCA stenosis or occlusion.

2. Materials and methods

2.1. Subjects

This study was approved by the Medical Ethics Committee of First Affiliated Hospital of Shandong First Medical University. All recruited participants provided their informed consent. Forty-six patients diagnosed with chronic unilateral MCA stenosis or occlusion and 38 age-, sex-, and education-matched healthy controls were recruited from September 2020 to June 2021. The clinical variables history of hypertension, diabetes, hyperlipidemia, hyperhomocysteinemia, smoking, and drinking were collected for all patients.

All enrolled patients were diagnosed by neurological experts based on clinical symptoms, conventional MRI, magnetic resonance angiography (MRA), or digital subtraction angiography. The inclusion criteria for patients with unilateral MCA stenosis or occlusion were as follows: 1) unilateral MCA stenosis or occlusion confirmed by imaging examination, with other large vessels showing no or only mild stenosis; 2) long-term ischemic attack symptoms associated with unilateral MCA stenosis or occlusion (the interval between the first symptom onset and the examination was $\geq$ 4 weeks); 3) complete clinical data and MR images without artifacts; and 4) no previous history of cerebral hemorrhage, brain tumor, brain injury, or dementia. The exclusion criteria of patients included 1) obvious stenosis or occlusion of other intracranial vessels; 2) acute embolic MCA stenosis or occlusion; 3) multiple sclerosis (MS), PD, AD, or other neurological diseases; 4) claustrophobia; 5) cardiac pacemakers or metal foreign bodies; and 6) severe artifacts on MR images. All healthy controls without cerebrovascular diseases had no brain injury, neurological, psychiatric, metabolic, or other systemic diseases that may affect the nervous system. Conventional MRI scans also showed no obvious abnormalities or only small lacunar infarcts. All participants were right-handed.

2.2. Imaging acquisition

MRI was performed on a 3.0-T MRI scanner (Discovery MR750, GE Healthcare, Chicago, IL, USA) equipped with a 32-channel phase-array head coil. In addition to conventional MRI of T1-weighted imaging (T1WI), T2WI, and T2 fluid-attenuated inversion recovery (T2-FLAIR), 3D time-of-flight (TOF)-MRA and QSM were also performed for each participant. The corresponding scan parameters were as follows:

T1WI: repetition time (TR)/echo time (TE) = 2965.2/24.0 ms, field-of-view (FOV) = 240 mm × 240 mm, matrix size = 320 × 160, slice thickness = 5 mm, number of slices = 22, scanning time = 46 s.

T2WI: TR/TE = 6182.0/102.0 ms, FOV = 240 mm × 240 mm, matrix size = 384 × 256, slice thickness = 5 mm, number of slices = 22, scanning time = 56 s.

T2-FLAIR: TR/TE = 8000/88.5 ms, FOV = 240 mm × 240 mm, matrix size = 320 × 256, slice thickness = 5 mm, number of slices = 22, scanning time = 1 min 44 s.

TOF-MRA: TR/TE = 21/2.5 ms, FOV = 220 mm × 88 mm, matrix size = 320 × 256, slice thickness = 1.6 mm, number of slices = 128, scanning time = 4 min 1 s.

3D spoiled gradient echo-based QSM imaging: number of TEs = 8, first TE = 3.0 ms, TE interval = 3.1 ms, TR = 28.1 ms, FOV = 240 mm × 240 mm, flip angle = 20°, matrix size = 240 × 240, slice thickness = 2 mm, number of slices = 64, scanning time = 2 min 31 s.

2.3. Imaging analysis

The STI Suite embedded in MATLAB (MathWorks, Natick, MA), as a widely used software for susceptibility analysis, was applied in this study for QSM susceptibility mapping calculations.(Li et al., 2014) The

corresponding susceptibility post-processing steps are briefly summarized as follows: first, unwrapped phase images were generated by Laplacian-based unwrapping algorithms.(Li et al., 2014) Second, sophisticated harmonic artifact reduction for phase data with the varying spherical kernel sizes (V-SHARP) method was used to remove inhomogeneity background fields.(Li et al., 2014) Finally, QSM images were obtained using the least-squares (LSQR)-algorithm-based method to calculate dipole inversion.(Li et al., 2015).

The obtained QSM-derived susceptibility maps, displayed using Image J software (National Institutes of Health, Bethesda, MD, USA), were used to draw regions-of-interest (ROIs) manually in the GM nucleus area, including in the bilateral CN, PU, GP, thalamus (TH), SN, red nucleus (RN), and dentate nucleus (DN), by two neuroradiologists (X.Y. W and H.M.M) with>3 years of experience. Both observers were blinded to the clinical and imaging information of all subjects. According to the anatomical structure of the GM nuclei, each ROI was drawn on continuous slices that could clearly show the boundary of the GM nuclei on QSM images (Fig. 1). Meanwhile, focal areas with infarcts were avoided. Mean susceptibility and the standard deviation of each ROI, as measured by the two observers, were obtained.

2.4. Statistical analysis

Normality of continuous variables was analyzed using the Kolmogorov-Smirnov test. Data that had a normal distribution are reported as mean ± standard deviation. Counting data are represented as frequency and percentage (%). Comparisons of clinical data between healthy controls and patients were performed using the independent sample *t*-test for age and education, and the chi-square (χ^2) test for counting data. The intra-class correlation coefficient (ICC) was used to evaluate the inter-observer agreement of susceptibility measurement between the two radiologists. An ICC > 0.75 was considered as showing good reproducibility.

Paired sample *t*-test was separately used to compare susceptibility between the left and right GM nuclei in healthy controls and the ipsilateral and contralateral GM nuclei in patients with unilateral MCA stenosis or occlusion. Independent sample *t*-test was performed to assess the susceptibility differences between healthy controls and the ipsilateral / contralateral sides of patients, respectively. If significantly different susceptibility was shown in any GM nucleus subregion between the right and left sides in healthy controls, the independent sample *t*-test was further used to compare susceptibility differences between the ipsilateral side of the patients and the corresponding side of the healthy controls for this subregion. To implement this, all 27 patients with right MCA stenosis or occlusion were selected from the patient group for simplicity and the correspondingly 27 normal subjects were randomly selected from the healthy control group. Receiver operating characteristic (ROC) curve analysis and area under the ROC curve (AUC) were used to evaluate the efficacy of QSM susceptibility in distinguishing patients with unilateral MCA stenosis or occlusion from healthy controls. Additionally, the GM nucleus subregions showing different susceptibilities between healthy controls and patients were further evaluated with multiple linear regression analysis, to assess the respective relationship of susceptibility levels with clinical variables. Due to not large sample size, variables with *P*-value < 0.1 obtained from univariate analysis were considered as independent variables for further multiple linear regression analysis.

All statistical analyses were performed in GraphPad Prism 8.0 (GraphPad Software, Inc., La Jolla, CA, USA) and IBM SPSS 22.0 (Armonk, NY, USA). $P < 0.05$ was considered the threshold of significance.

3. Results

3.1. Demographic information of all participants

Forty-six patients with unilateral MCA stenosis or occlusion (24 males and 22 females; average age: 52.35 ± 11.82 years; average education: 10.70 ± 3.20 years) and 38 healthy controls (16 males and 22 females; average age: 48.50 ± 14.16 years; average education: 11.39 ± 3.39 years) were recruited in this study. Among all patients, 19 and 27 patients had left MCA stenosis/occlusion and right MCA stenosis/occlusion, respectively. No significant differences were noted between the patient and healthy control groups in terms of age, sex, and education level ($P = 0.179$; $P = 0.358$; $P = 0.335$, respectively). The detailed clinical characteristics of all subjects are summarized in Table 1.

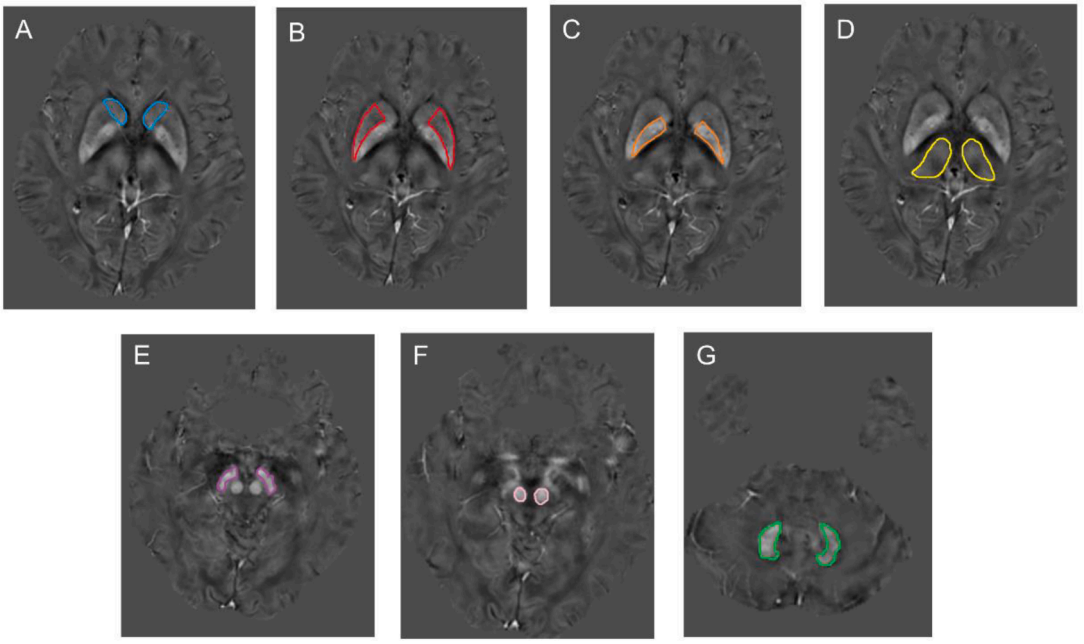

Fig. 1. Regions-of-interest (ROIs) depicted on quantitative susceptibility mapping (QSM) images. A. Bilateral caudate nucleus (CN); B. bilateral putamen (PU); C. bilateral globus pallidus (GP); D. bilateral thalamus (TH); E. bilateral substantia nigra (SN); F. bilateral red nucleus (RN); G. bilateral dentate nucleus (DN). (For interpretation of the references to colour in this figure legend, the reader is referred to the web version of this article.)

Table 1
Demographic information of all participants.

	Healthy control group (n = 38)	Patient Group (n = 46)	*P*-value
Age (years)	48.50 ± 14.16	52.35 ± 11.82	0.179
Sex (male)	16 (42.11%)	24 (52.71%)	0.358
Education (years)	11.39 ± 3.39	10.70 ± 3.20	0.335
Location of lesion (right)	–	27 (58.70%)	–
Disease duration (years)	–	2.22 ± 2.39	–
Hypertension	4 (10.53%)	33 (71.74%)	0.000
Diabetes	2 (5.26%)	15 (32.61%)	0.002
Hyperlipidemia	–	15 (32.61%)	–
Hyperhomocysteinemia	–	12 (26.09%)	–
History of smoking	3 (7.89%)	13 (28.26%)	0.018
History of drinking	3 (7.89%)	13 (28.26%)	0.018

–, not significant or not measured.

3.2. Analysis of Inter-observer agreement for susceptibility measurement

Using the ICC analysis, high inter-observer agreements between the two radiologists were confirmed by the high ICC values ($0.811 \leq ICCs \leq 0.939$, Table 2) for susceptibility measurement in all seven GM nucleus subregions.

3.3. Susceptibility comparisons between the bilateral GM nucleus subregions of healthy controls

Using the paired *t*-test, comparable levels of susceptibility were shown between the bilateral PU, GP, TH, SN, RN and DN, separately, for healthy controls. However, significantly different susceptibility was found in the left and right CN (mean: 0.0299 ± 0.01023 ppm ($\times 10^{-6}$) vs. 0.0282 ± 0.00956 ppm ($\times 10^{-6}$); $P = 0.046$, Table 3).

3.4. Susceptibility comparisons between the ipsilateral and contralateral GM nucleus subregions of patients with unilateral MCA stenosis or occlusion

Using paired sample *t*-test, comparable susceptibility was separately found in the CN, TH, RN, and DN between the ipsilateral and contralateral sides of patients (all $P > 0.05$, Table 4). However, the ipsilateral side to lesion exhibited significantly higher susceptibility than the contralateral side in the PU, GP, and SN ($P < 0.05$; Table 4 **and** Fig. 2).

3.5. Susceptibility comparisons of GM nucleus subregions between patients and healthy controls

Except for the CN, most GM nucleus subregions showed comparable susceptibility between the left and right ROI in healthy controls (Table 3). Therefore, the mean of the left and right susceptibility for each pair of GM nuclei in healthy controls was used in further statistical analyses.

With independent sample *t*-test, compared with healthy controls, the ipsilateral side of patients also presented significantly increased susceptibility in the PU, GP, and SN ($P < 0.05$; Table 5 **and** Fig. 3), while comparable susceptibility was found in the CN, TH, RN, and DN between both groups (all $P > 0.05$, Table 5).

Independent sample *t*-test also showed no significant differences of susceptibility in the CN, GP, TH, SN, RN, and DN between healthy controls and the contralateral side of patients (all $P > 0.05$, Table 6). However, the susceptibility of PU in the contralateral side of patients was significantly higher than in healthy controls ($P < 0.05$; Table 6 **and** Fig. 4).

Significantly different susceptibility was shown between the left and right CN in healthy controls ($P < 0.05$; Table 3). To investigate this discrepancy in the CN region, an independent sample *t*-test was additionally implemented to compare the susceptibility of the CN region between the right side (ipsilateral to the lesion) in 27 patients with right MCA stenosis/occlusion (11 males and 16 females; average age: 50.41 ± 13.92 years; average education: 10.89 ± 3.38 years) and the right side in 27 healthy controls (11 males and 16 females; average age: 49.37 ± 13.81 years; average education: 10.74 ± 3.33 years). No significant differences were noted in age, sex, or education level ($P = 0.784$; $P > 0.999$; $P = 0.872$, respectively); additionally, no differences in susceptibility in the right CN were found between these two groups ($P > 0.05$, Table 7).

3.6. ROC curve analysis of QSM-derived susceptibility in the diagnosis of unilateral MCA stenosis or occlusion

The GM nucleus subregions of the PU, GP, and SN on the ipsilateral side, which showed significantly different susceptibility from healthy controls (Table 5 **and** Fig. 3), were further investigated for the efficacy of QSM-derived susceptibility to differentiate patients with unilateral MCA stenosis or occlusion from healthy controls. Using the ROC analysis, the highest AUC value was obtained for the PU (AUC = 0.773, $P < 0.05$), as compared with the GP or SN (AUC = 0.662 and 0.681, both $P < 0.05$) (Fig. 5). The corresponding sensitivity, specificity, and cutoff

Table 2
ICC of agreement between the two radiologists for susceptibility measurement.

ROI	ICC for the healthy control group		ICC for the patient group	
	Left	Right	Ipsilateral side	Contralateral side
CN	0.891	0.853	0.811	0.915
PU	0.921	0.866	0.938	0.869
GP	0.924	0.936	0.899	0.923
TH	0.896	0.885	0.853	0.833
SN	0.826	0.909	0.893	0.939
RN	0.914	0.897	0.931	0.882
DN	0.812	0.879	0.885	0.816

ICC, intra-class correlation coefficient; ROI, region-of-interest; CN, caudate nucleus; PU, putamen; GP, globus pallidus; TH, thalamus; SN, substantia nigra; RN, red nucleus; DN, dentate nucleus.

Table 3
Susceptibility [ppm ($\times 10^{-6}$)] comparisons between the bilateral gray matter nuclei in healthy controls.

ROI	Left (n = 38)	Right (n = 38)	*t* -value	*P*-value
CN	0.0299 ± 0.01023	0.0282 ± 0.00956	2.069	0.046
PU	0.0394 ± 0.01240	0.0389 ± 0.01378	0.535	0.596
GP	0.0843 ± 0.01960	0.0854 ± 0.01860	−0.737	0.466
TH	0.0148 ± 0.00407	0.0150 ± 0.00448	−0.656	0.516
SN	0.0873 ± 0.02158	0.0919 ± 0.02417	−1.973	0.056
RN	0.0765 ± 0.02857	0.0753 ± 0.02637	0.626	0.535
DN	0.0676 ± 0.02035	0.0668 ± 0.02184	0.493	0.625

ROI, region-of-interest; CN, caudate nucleus; PU, putamen; GP, globus pallidus; TH, thalamus; SN, substantia nigra; RN, red nucleus; DN, dentate nucleus.

Table 4
Susceptibility [ppm ($\times 10^{-6}$)] comparisons in gray matter nucleus subregions between the ipsilateral and contralateral sides in patients with unilateral MCA stenosis or occlusion.

ROI	Ipsilateral side (n = 46)	Contralateral side (n = 46)	*t-value*	*P-value*
CN	0.0319 ± 0.00903	0.0305 ± 0.00992	1.155	0.254
PU	0.0581 ± 0.02279	0.0466 ± 0.01406	5.233	<0.000
GP	0.0984 ± 0.02696	0.0900 ± 0.0256	4.133	0.000
TH	0.0141 ± 0.01408	0.0137 ± 0.00508	0.715	0.478
SN	0.1051 ± 0.02500	0.0972 ± 0.02547	3.444	0.001
RN	0.0849 ± 0.02729	0.0835 ± 0.02451	0.745	0.460
DN	0.0681 ± 0.02565	0.0678 ± 0.02011	0.204	0.839

MCA, middle cerebral artery; ROI, region-of-interest; CN, caudate nucleus; PU, putamen; GP, globus pallidus; TH, thalamus; SN, substantia nigra; RN, red nucleus; DN, dentate nucleus.

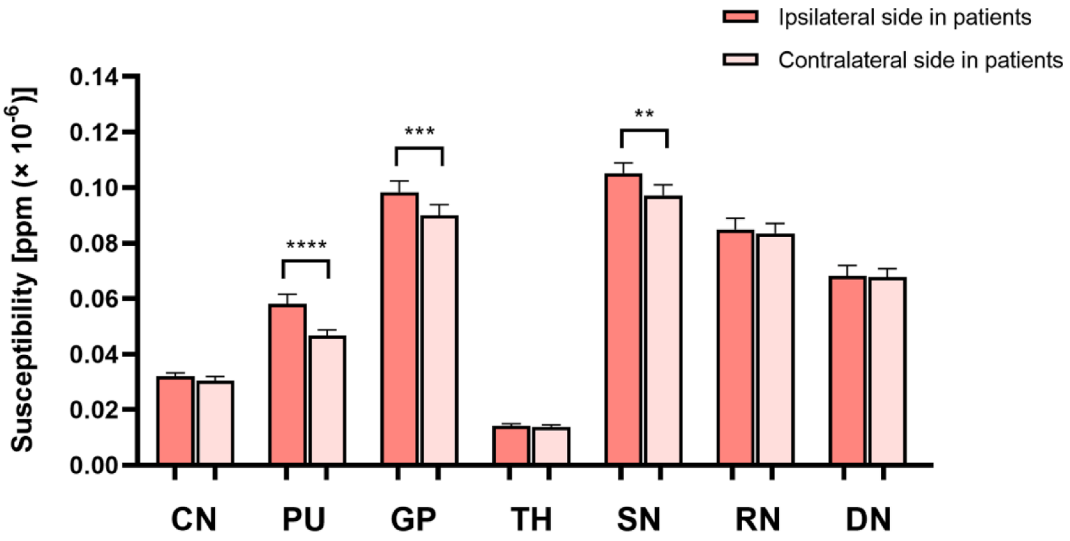

Fig. 2. Bar diagrams showing comparisons of the susceptibility of seven gray matter nucleus subregions between the ipsilateral and contralateral sides of patients with unilateral MCA stenosis or occlusion. Significant difference: **, $P < 0.01$; ***, $P < 0.001$; ****, $P < 0.0001$.

Table 5
Susceptibility [ppm ($\times 10^{-6}$)] comparisons in gray matter nucleus subregions between healthy controls and the ipsilateral side in patients with unilateral MCA stenosis or occlusion.

ROI	Healthy controls (n = 38)	Ipsilateral side in patients (n = 46)	*t-value*	*P-value*
CN	0.0290 ± 0.00954	0.0319 ± 0.00903	−1.411	0.162
PU	0.0392 ± 0.01284	0.0581 ± 0.02279	−4.554	<0.000
GP	0.0849 ± 0.01859	0.0984 ± 0.02696	−2.615	0.011
TH	0.0149 ± 0.00408	0.0141 ± 0.01408	0.780	0.437
SN	0.0896 ± 0.02178	0.1051 ± 0.02500	−2.970	0.004
RN	0.0759 ± 0.02689	0.0849 ± 0.02729	−1.510	0.135
DN	0.0672 ± 0.02054	0.0681 ± 0.02565	−0.169	0.866

MCA, middle cerebral artery; ROI, region-of-interest; CN, caudate nucleus; PU, putamen; GP, globus pallidus; TH, thalamus; SN, substantia nigra; RN, red nucleus; DN, dentate nucleus.

values were 60.87%, 81.58%, and 0.0486 ppm ($\times 10^{-6}$) for the ipsilateral PU; 71.74%, 65.79%, and 0.0858 ppm ($\times 10^{-6}$) for the ipsilateral GP; and 73.91%, 63.16%, and 0.0949 ppm ($\times 10^{-6}$) for the ipsilateral SN, respectively.

3.7. Association between the ipsilateral susceptibility and clinical variables

Additionally, multiple linear regression analysis was further used to

Table 6
Susceptibility [ppm ($\times 10^{-6}$)] comparisons in gray matter nucleus subregions between healthy controls and the contralateral side in patients with unilateral MCA stenosis or occlusion.

ROI	Healthy controls (n = 38)	Contralateral side in patients (n = 46)	*t-value*	*P-value*
CN	0.0290 ± 0.00954	0.0305 ± 0.00992	−0.665	0.508
PU	0.0392 ± 0.01284	0.0466 ± 0.01406	−2.511	0.014
GP	0.0849 ± 0.01859	0.0900 ± 0.0256	−1.033	0.305
TH	0.0149 ± 0.00408	0.0137 ± 0.00508	1.126	0.263
SN	0.0896 ± 0.02178	0.0972 ± 0.02547	−1.450	0.151
RN	0.0759 ± 0.02689	0.0835 ± 0.02451	−1.352	0.180
DN	0.0672 ± 0.02054	0.0678 ± 0.02011	−0.120	0.905

MCA, middle cerebral artery; ROI, region-of-interest; CN, caudate nucleus; PU, putamen; GP, globus pallidus; TH, thalamus; SN, substantia nigra; RN, red nucleus; DN, dentate nucleus.

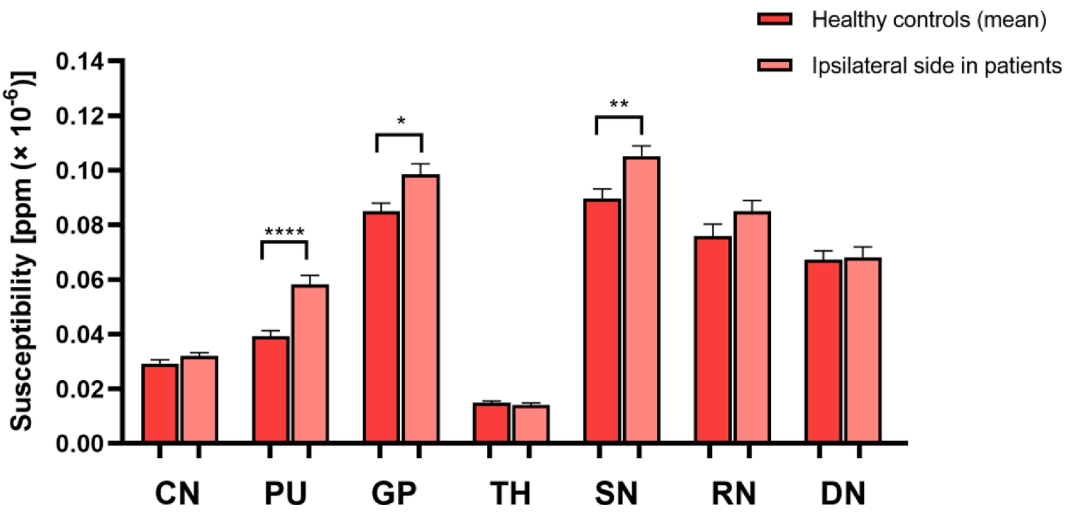

Fig. 3. Bar diagrams showing comparisons of the susceptibility of seven gray matter nucleus subregions between healthy controls and the ipsilateral side of patients with unilateral MCA stenosis or occlusion. Significant difference: *, $P < 0.05$; **, $P < 0.01$; ****, $P < 0.0001$.

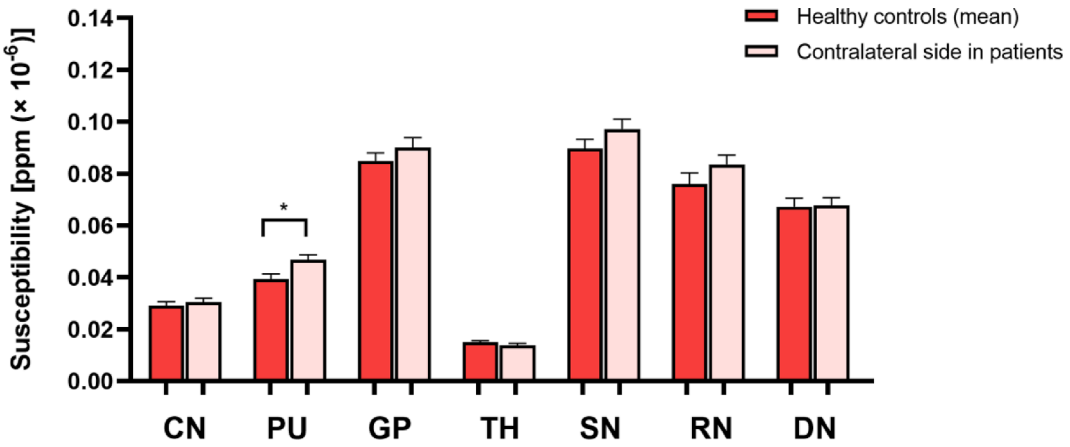

Fig. 4. Bar diagrams showing comparisons of the susceptibility of seven gray matter nucleus subregions between healthy controls and the contralateral side of patients with unilateral MCA stenosis or occlusion. Significant difference: *, $P < 0.05$.

Table 7
Susceptibility [ppm ($\times 10^{-6}$)] comparison between 27 healthy controls and all 27 patients with right MCA stenosis or occlusion in the right CN.

ROI	Healthy controls (n = 27)	Right MCA stenosis or occlusion (n = 27)	*t*-value	*P*-value
Right CN	0.0276 ± 0.00897	0.0312 ± 0.00973	1.33	0.189

MCA, middle cerebral artery; CN, caudate nucleus; ROI, region-of-interest.

assess the respective relationship of the susceptibility levels in these three nucleus subregions on the ipsilateral side (lesion side PU, GP, and SN) with clinical variables. First, in univariate analysis, age, hypertension and diabetes were associated with increased susceptibility values in these three regions, smoking was relevant to the susceptibility levels in the ipsilateral GP and SN, and hyperlipidemia was associated with increased susceptibility values in the ipsilateral GP (all $P < 0.1$; Table 8). Therefore, these variables were further applied for the subsequent multiple linear regression analysis.

Multiple linear regression results showed that patients with hypertension exhibited significantly higher susceptibility in the ipsilateral PU ($\beta = 0.017$, $P = 0.017$), and with smoking exhibited significantly higher susceptibility in the ipsilateral GP ($\beta = 0.022$, $P = 0.019$). Moreover, diabetes-related increase in susceptibility was observed in the ipsilateral SN ($\beta = 0.025$, $P = 0.002$). Details of the multiple linear regression analysis are listed in Table 9.

4. Discussion

In this study, QSM-derived susceptibility was used to investigate potential changes in the iron content in the deep GM nuclei of patients with long-term cerebral ischemia caused by unilateral MCA stenosis or occlusion. As shown in the results, the ipsilateral PU, GP, and SN presented significantly increased susceptibility in patients with long-term unilateral MCA stenosis or occlusion compared with healthy controls, and the ipsilateral PU, GP, and SN also exhibited significantly higher

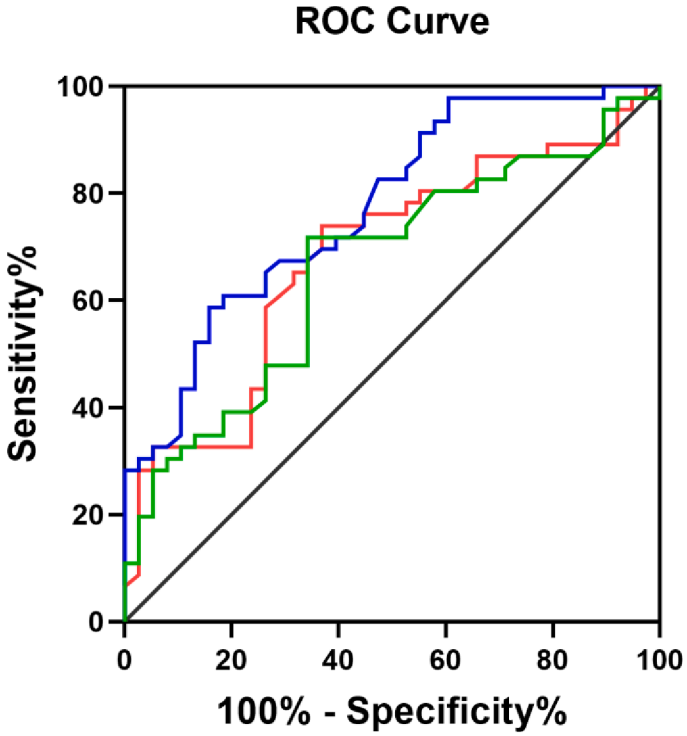

Fig. 5. Receiver operating characteristic (ROC) curve showing the efficacy of the susceptibility in the ipsilateral side putamen (PU), globus pallidus (GP), and substantia nigra (SN) in differentiating unilateral middle cerebral artery stenosis or occlusion patients from healthy controls. The highest area under the ROC curve (AUC) value was found on the ipsilateral PU (AUC = 0.773, $P < 0.05$), relative to the GP and SN (AUC = 0.662 and 0.681, both $P < 0.05$). The corresponding sensitivity, specificity, and cutoff values were 60.87%, 81.58%, and 0.0486 ppm ($\times 10^{-6}$) for the ipsilateral PU; 71.74%, 65.79%, and 0.0858 ppm ($\times 10^{-6}$) for the ipsilateral GP; and 73.91%, 63.16%, and 0.0949 ppm ($\times 10^{-6}$) for the ipsilateral SN, respectively.

Table 8
Univariate analysis of clinical variables relevant to susceptibility levels on the ipsilateral PU, GP, and SN in patients with unilateral MCA stenosis or occlusion.

Variables	Ipsilateral PU		Ipsilateral GP		Ipsilateral SN	
	β	*P-value*	*β*	*P-value*	*β*	*P-value*
Age (years)	0.001	0.013	0.001	0.069	0.001	0.049
Comorbidity present (vs not present)						
Hypertension	0.021	0.004	0.017	0.051	0.015	0.015
Diabetes	0.012	0.086	0.015	0.082	0.030	0.000
Hyperlipidemia	0.001	0.908	0.015	0.087	0.007	0.357
Hyperhomocysteinemia	−0.005	0.485	−0.010	0.299	−0.006	0.463
Smoking	0.002	0.790	0.020	0.022	0.015	0.065
Drinking	−0.005	0.490	0.014	0.102	0.006	0.449

PU, putamen; GP, globus pallidus; SN, substantia nigra; MCA, middle cerebral artery.

Table 9
Multiple linear regression analysis of clinical variables relevant to susceptibility levels on the ipsilateral PU, GP, and SN in patients with unilateral MCA stenosis or occlusion.

	Variables	*β*	*t*	*p*	Adjusted R^2 of model	*F* of model	*P* of model
Ipsilateral PU	Age (years)	0.000	1.754	0.087	0.214	5.080	0.004
	Hypertension	0.017	2.493	0.017			
	Diabetes	0.006	0.937	0.354			
Ipsilateral GP	Age (years)	0.001	1.809	0.078	0.214	3.451	0.011
	Hypertension	0.005	0.612	0.544			
	Diabetes	0.002	0.198	0.844			
	Hyperlipidemia	0.015	1.956	0.057			
	Smoking	0.022	2.434	0.019			
Ipsilateral SN	Age (years)	0.000	0.861	0.394	0.337	6.713	0.000
	Hypertension	0.012	1.701	0.097			
	Diabetes	0.025	3.381	0.002			
	Smoking	0.005	0.657	0.515			

PU, putamen; GP, globus pallidus; SN, substantia nigra; MCA, middle cerebral artery.

susceptibility than the contralateral side in patients. In addition, susceptibility of the contralateral PU of patients was significantly higher than in healthy controls. Using the ROC analysis, a high AUC value was identified for susceptibility in the ipsilateral PU, indicating that QSM susceptibility could robustly distinguish patients with unilateral MCA stenosis or occlusion from healthy controls. Furthermore, regression analysis revealed significant associations of the ipsilateral PU, GP, and SN susceptibility with certain clinical variables, including hypertension, smoking, and diabetes.

While a pathological test for iron quantification has limited clinical application, mainly due to its intrinsic invasiveness, QSM susceptibility has here been demonstrated to be an effective quantitative indicator of iron measurement. Previous studies have confirmed that QSM susceptibility correlated positively with the average iron levels in brain tissue. (Langkammer et al., 2012; Sun et al., 2015) Moreover, QSM has been able to identify iron metabolism disorders in the brain, particularly in GM nuclei, for neurological diseases such as AD, MS, PD, and HD. (Domínguez D et al., 2016; Du et al., 2016; He et al., 2015; Schweser et al., 2021; Acosta-Cabronero et al., 2013) With these promising results, QSM can thus be considered a reliable, noninvasive method for the quantitative investigation of iron alterations in GM nuclei for patients with cerebral ischemia.

In this study, iron-related susceptibility of the ipsilateral PU, GP, and SN and of the contralateral PU were significantly higher in patients with unilateral MCA stenosis or occlusion than in healthy controls, indicating that abnormal iron deposition may be present in the brain after long-term cerebral ischemia. In addition, for patients, the PU, GP, and SN also exhibited significantly higher susceptibility on the ipsilateral than contralateral side, suggesting that specific GM nucleus subregions ipsilateral to the lesion were more vulnerable to increased iron deposition after long-term focal cerebral ischemia. Similar to our finding, Du et al. (Du et al., 2020) also reported that the average QSM susceptibility of the bilateral PU in nine patients with unilateral MCA occlusion was significantly higher than that in healthy controls. However, for bilateral GP regions, lower average susceptibility was revealed in patients than in healthy controls. There were no significant susceptibility differences between the ipsilateral and contralateral sides in all focused regions of interest, including CN, PU, and GP for these nine patients, which are not consistent with our finding. The possible reasons for this discrepancy include that different patient types were recruited in the two studies. Du et al. only focused on unilateral MCA occlusion. Furthermore, Du et al.'s study involved fewer patients than those included in the present study (9 vs. 46), which potentially introduces statistical bias, limiting the reproducibility of the finding. This might also be why comparable susceptibility in the bilateral PU and GP was found in their study in patients and healthy controls. Therefore, follow-up research with a large clinical cohort is warranted to confirm this.

The GM nucleus subregions of the ipsilateral PU, GP, and SN, which showed significantly different susceptibility, were further investigated for efficacy in differentiating patients with unilateral MCA stenosis or occlusion from healthy controls using ROC analysis. A high AUC value was identified for susceptibility in the ipsilateral PU, indicating that QSM susceptibility could distinguish patients with unilateral MCA stenosis or occlusion from healthy controls. QSM may thus be a noninvasive technique to evaluate changes in the cerebral iron content in patients after long-term cerebral ischemia.

In addition, we further evaluated the respective relationship of susceptibility levels of the ipsilateral PU, GP, and SN with common risk factor variables for intracranial artery stenosis or occlusion, including a history of hypertension, diabetes, hyperlipidemia, hyperhomocysteinemia, smoking, and drinking. In addition, age was included in further multiple linear regression analysis, as this variable revealed association with increased susceptibility in these three subregions in our univariate analysis and also reported in the literature (Li et al., 2014;

Gong et al., 2015). Hypertension-related iron deposition was observed in the ipsilateral PU; smoking-related iron deposition was found in the GP; and diabetes-related iron deposition was found in the SN. Rodrigue et al. (Rodrigue et al., 2011) pointed out that the iron content, evaluated by T2*-weighted imaging in all examined regions, including the CN, PU, primary visual cortex, hippocampus, prefrontal cortex, and entorhinal cortex, was significantly increased in hypertensive subjects. Previously, QSM was used to study the characteristics of iron deposition in GM nucleus subregions in older people, which revealed that older individuals with a history of smoking had increased iron content in the TH. (Li et al., 2021) Another study suggested that mean QSM susceptibility of the bilateral PU was significantly increased in patients with type 2 diabetes.(Li et al., 2020) Together with these previous results, our findings indicated that high risk factors for common cerebrovascular diseases may lead to changes of iron content in the brain, and different factors cause variable patterns of iron deposition. Some risk factors for intracranial artery stenosis may aggravate increased iron deposition after long-term cerebral ischemia.

Our results suggested that the iron content in specific GM nucleus regions increases after long-term cerebral ischemia. Iron is an essential element in normal neurophysiological functions in the brain. Normal iron metabolism and the balance in cerebral iron play an important role in the functional activities of the brain. However, iron overload caused by iron homeostasis imbalance can lead to various neurodegenerative diseases.(Thirupathi and Chang, 2019) In ischemic stroke, glutamate excitotoxicity, oxidative stress, non-infectious neuroinflammation, and so on can cause neuronal death in the corresponding long-term ischemic area.(Nagy and Nardai, 2017) Oxidative stress induced by free radicals is an important pathogenic factor of ischemia/reperfusion injury. The most harmful free radical, the hydroxyl radical, is produced through an iron-catalyzed reaction, and iron overload is the main cause of oxidative stress in ischemic brain tissue.(Liu et al., 2020) In addition, intracellular iron overload is the key to ferroptosis, which is a new type of regulatory cell death mainly induced by iron-dependent lipid peroxidation. (Hirschhorn and Stockwell, 2019) Several studies have found that ferroptosis is becoming an important mechanism of pathological cell death during ischemic stroke and other brain injuries (DeGregorio-Rocasolano et al., 2019; Weiland et al., 2019). Moreover, iron overload exacerbates the risk of hemorrhagic transformation after ischemic stroke (García-Yébenes et al., 2018). A clinical study has reported that high serum ferritin levels weaken the beneficial effects of thrombolytic therapy in patients with ischemic stroke (Millan et al., 2007). However, the inhibition of iron overload can reduce stroke injury. Numerous preclinical experiments have shown that the use of iron chelators in animal models of ischemic stroke can reduce the formation of free radicals and lipid peroxidation, thereby reducing mortality, infarct volume, brain swelling, and the risk of hemorrhagic transformation in ischemic stroke (Hanafy et al., 2019; Kosyakovsky et al., 2021).

Currently, research focusing on the toxic effect of iron overload on patients with ischemic stroke and the effect of iron chelators in clinical stroke patients is still at an early stage. Several preclinical experiments and early clinical data have shown that iron chelators play a beneficial role in the treatment of several neurological diseases, including AD, PD, ischemic stroke, and intracranial hemorrhage.(Hanafy et al., 2019; Kosyakovsky et al., 2021) Drugs targeting the regulation of brain iron are expected to become potential effective treatments after ischemic stroke. In addition, common cerebrovascular risk factors should be controlled through lifestyle changes or medication, as these factors not only cause intracranial atherosclerosis but may also exaggerate the increase in cerebral iron deposition after long-term cerebral ischemia.

This study had some limitations. First, this was a single-center study with a limited number of patients enrolled, which may have introduced potential selection bias. Second, the dynamic relationship between cerebral ischemia and variations in iron content in the GM nuclei was not investigated in this study. Third, more detailed clinical data, for instance, smoking dosage or severity factor, were not fully recorded in this study. To address these issues, further prospective, longitudinal studies with a larger clinical cohort and comprehensive clinical records are needed.

5. Conclusions

In conclusion, with QSM imaging, patients with long-term unilateral MCA stenosis or occlusion showed increased iron deposition in the PU, GP, and SN regions on the side ipsilateral to the lesion. Some cerebrovascular disease risk factors, including hypertension, diabetes, and smoking, may aggravate increased iron deposition after long-term cerebral ischemia. These findings indicated that cerebral iron metabolism disorders may exist after chronic MCA stenosis or occlusion. Therefore, increased iron deposition in the GM nuclei, as measured by QSM, may be a potential biomarker for long-term cerebral ischemia.

CRediT authorship contribution statement

Huimin Mao: Conceptualization, Data curation, Formal analysis, Investigation, Validation, Visualization, Writing – original draft, Writing – review & editing. **Weiqiang Dou:** Conceptualization, Data curation, Formal analysis, Investigation, Validation, Visualization, Writing – original draft, Writing – review & editing. **Kunjian Chen:** Software, Methodology. **Xinyu Wang:** Investigation, Validation. **Xinyi Wang:** Conceptualization, Funding acquisition, Supervision, Writing – original draft, Writing – review & editing. **Yu Guo:** Resources, Data curation. **Chao Zhang:** Resources, Methodology.

Acknowledgment

The study was supported by Shandong Science and Technology Development Plan Project 2009GG10002024.

References

Kuriakose, D., Xiao, Z., 2020. Pathophysiology and treatment of stroke: present status and future perspectives. Int. J. Mol. Sci. 21, 7609. https://doi.org/10.3390/ijms21207609.

Ran, Y., Wang, Y., Zhu, M., Wu, X., Malhotra, A., Lei, X., Zhang, F., Wang, X., Xie, S., Zhou, J., Zhu, J., Cheng, J., Zhu, C., 2020. Higher plaque burden of middle cerebral artery is associated with recurrent ischemic stroke: A quantitative magnetic resonance imaging study. Stroke 51 (2), 659–662.

Sekerdag, E., Solaroglu, I., Gursoy-Ozdemir, Y., 2018. Cell death mechanisms in stroke and novel molecular and cellular treatment options. Curr. Neuropharmacol. 16, 1396–1415. https://doi.org/10.2174/1570159X16666180302115544.

Connor, J.R., Menzies, S.L., Burdo, J.R., Boyer, P.J., 2001. Iron and iron management proteins in neurobiology. Pediatr. Neurol. 25, 118–129. https://doi.org/10.1016/s0887-8994(01)00303-4.

Hubler, M.J., Peterson, K.R., Hasty, A.H., 2015. Iron homeostasis: A new job for macrophages in adipose tissue? Trends Endocrinol. Metab. 26, 101–109. https://doi.org/10.1016/j.tem.2014.12.005.

Apostolakis, S., Kypraiou, A.M., 2017. Iron in neurodegenerative disorders: Being in the wrong place at the wrong time? Rev. Neurosci. 28, 893–911. https://doi.org/10.1515/revneuro-2017-0020.

Stankiewicz, J., Panter, S.S., Neema, M., Arora, A., Batt, C.E., Bakshi, R., 2007. Iron in chronic brain disorders: imaging and neurotherapeutic implications. Neurotherapeutics. 4, 371–386. https://doi.org/10.1016/j.nurt.2007.05.006.

Hayflick, S.J., Kurian, M.A., Hogarth, P., 2018. Neurodegeneration with brain iron accumulation. Handb Clin Neurol. 147, 293–305. https://doi.org/10.1016/B978-0-444-63233-3.00019-1.

Tuo, Q.-z., Lei, P., Jackman, K.A., Li, X.-l., Xiong, H., Li, X.-l., Liuyang, Z.-y., Roisman, L., Zhang, S.-t., Ayton, S., Wang, Q., Crouch, P.J., Ganio, K., Wang, X.-c., Pei, L., Adlard, P.A., Lu, Y.-m., Cappai, R., Wang, J.-z., Liu, R., Bush, A.I., 2017. Tau-mediated iron export prevents ferroptotic damage after ischemic stroke. Mol. Psychiatry 22 (11), 1520–1530.

Dietrich, R.B., Bradley Jr., W.G., 1988. Iron accumulation in the basal ganglia following severe ischemic-anoxic insults in children. Radiology 168, 203–206. https://doi.org/10.1148/radiology.168.1.3380958.

Vinayagamani, S., Sheelakumari, R., Sabarish, S., Senthilvelan, S., Ros, R., Thomas, B., Kesavadas, C., 2021. Quantitative susceptibility mapping: Technical considerations and clinical applications in neuroimaging. J. Magn. Reson. Imaging 53 (1), 23–37.

Langkammer, C., Schweser, F., Krebs, N., Deistung, A., Goessler, W., Scheurer, E., Sommer, K., Reishofer, G., Yen, K., Fazekas, F., Ropele, S., Reichenbach, J.R., 2012. Quantitative susceptibility mapping (qsm) as a means to measure brain iron? A post mortem validation study. Neuroimage. 62 (3), 1593–1599.

Haacke, E.M., Liu, S., Buch, S., Zheng, W., Wu, D., Ye, Y., 2015. Quantitative susceptibility mapping: Current status and future directions. Magn. Reson. Imaging 33, 1–25. https://doi.org/10.1016/j.mri.2014.09.004.

Acosta-Cabronero J, Williams GB, Cardenas-Blanco A, Arnold RJ, Lupson V, Nestor PJ. In vivo quantitative susceptibility mapping (qsm) in alzheimer's disease. *PLoS One*. 2013;8:e81093. doi: 10.1371/journal.pone.0081093.

Du, G., Liu, T., Lewis, M.M., Kong, L., Wang, Y.i., Connor, J., Mailman, R.B., Huang, X., 2016. Quantitative susceptibility mapping of the midbrain in parkinson's disease. Mov. Disord. 31 (3), 317–324.

He, N., Ling, H., Ding, B., Huang, J., Zhang, Y., Zhang, Z., Liu, C., Chen, K., Yan, F., 2015. Region-specific disturbed iron distribution in early idiopathic parkinson's disease measured by quantitative susceptibility mapping. Hum. Brain Mapp. 36 (11), 4407–4420.

Domínguez D, J.F., Ng, A.C.L., Poudel, G., Stout, J.C., Churchyard, A., Chua, P., Egan, G. F., Georgiou-Karistianis, N., 2016. Iron accumulation in the basal ganglia in huntington's disease: Cross-sectional data from the image-hd study. J. Neurol. Neurosurg. Psychiatry 87 (5), 545–549.

Li, W., Avram, A.V., Wu, B., Xiao, X., Liu, C., 2014. Integrated laplacian-based phase unwrapping and background phase removal for quantitative susceptibility mapping. NMR Biomed. 27, 219–227. https://doi.org/10.1002/nbm.3056.

Li, W., Wang, N., Yu, F., Han, H., Cao, W., Romero, R., Tantiwongkosi, B., Duong, T.Q., Liu, C., 2015. A method for estimating and removing streaking artifacts in quantitative susceptibility mapping. Neuroimage. 108, 111–122.

Sun, H., Walsh, A.J., Lebel, R.M., Blevins, G., Catz, I., Lu, J.-Q., Johnson, E.S., Emery, D. J., Warren, K.G., Wilman, A.H., 2015. Validation of quantitative susceptibility mapping with perls' iron staining for subcortical gray matter. Neuroimage. 105, 486–492.

Schweser, F., Hagemeier, J., Dwyer, M.G., Bergsland, N., Hametner, S., Weinstock-Guttman, B., et al., 2021. Decreasing brain iron in multiple sclerosis: The difference between concentration and content in iron mri. Hum. Brain Mapp. 42, 1463–1474. https://doi.org/10.1002/hbm.25306.

Du, L., Zhao, Z., Liu, X., Chen, Y., Gao, W., Wang, Y., Liu, J., Liu, B., Ma, G., 2020. Alterations of iron level in the bilateral basal ganglia region in patients with middle cerebral artery occlusion. Front. Neurosci. 14, 608058 https://doi.org/10.3389/fnins.2020.608058.

Li, W., Wu, B., Batrachenko, A., Bancroft-Wu, V., Morey, R.A., Shashi, V., Langkammer, C., De Bellis, M.D., Ropele, S., Song, A.W., Liu, C., 2014. Differential developmental trajectories of magnetic susceptibility in human brain gray and white matter over the lifespan. Hum. Brain Mapp. 35 (6), 2698–2713.

Gong, N.J., Wong, C.S., Hui, E.S., Chan, C.C., Leung, L.M., 2015. Hemisphere, gender and age-related effects on iron deposition in deep gray matter revealed by quantitative susceptibility mapping. NMR Biomed. 28, 1267–1274. https://doi.org/10.1002/nbm.3366.

Rodrigue, K.M., Haacke, E.M., Raz, N., 2011. Differential effects of age and history of hypertension on regional brain volumes and iron. Neuroimage 54, 750–759. https://doi.org/10.1016/j.neuroimage.2010.09.068.

Li, J., Zhang, Q., Che, Y., Zhang, N., Guo, L., 2021. Iron deposition characteristics of deep gray matter in elderly individuals in the community revealed by quantitative susceptibility mapping and multiple factor analysis. Front. Aging Neurosci. 13, 611891 https://doi.org/10.3389/fnagi.2021.611891.

Li, J., Zhang, Q., Zhang, N., Guo, L., 2020. Increased brain iron deposition in the putamen in patients with type 2 diabetes mellitus detected by quantitative susceptibility mapping. J. Diabetes Res. 2020, 7242530. https://doi.org/10.1155/2020/7242530.

Thirupathi, A., Chang, Y.Z., 2019. Brain iron metabolism and cns diseases. Adv. Exp. Med. Biol. 1173, 1–19. https://doi.org/10.1007/978-981-13-9589-5_1.

Nagy, Z., Nardai, S., 2017. Cerebral ischemia/repefusion injury: From bench space to bedside. Brain Res. Bull. 134, 30–37. https://doi.org/10.1016/j.brainresbull.2017.06.011.

Liu, J., Guo, Z.N., Yan, X.L., Huang, S., Ren, J.X., Luo, Y., et al., 2020. Crosstalk between autophagy and ferroptosis and its putative role in ischemic stroke. Front. Cell. Neurosci. 14, 577403 https://doi.org/10.3389/fncel.2020.577403.

Hirschhorn, T., Stockwell, B.R., 2019. The development of the concept of ferroptosis. Free Radic Biol. Med. 133, 130–143. https://doi.org/10.1016/j.freeradbiomed.2018.09.043.

DeGregorio-Rocasolano, N., Marti-Sistac, O., Gasull, T., 2019. Deciphering the iron side of stroke: Neurodegeneration at the crossroads between iron dyshomeostasis, excitotoxicity, and ferroptosis. Front. Neurosci. 13, 85. https://doi.org/10.3389/fnins.2019.00085.

Weiland, A., Wang, Y., Wu, W., Lan, X.i., Han, X., Li, Q., Wang, J., 2019. Ferroptosis and its role in diverse brain diseases. Mol. Neurobiol. 56 (7), 4880–4893.

García-Yébenes, I., García-Culebras, A., Peña-Martínez, C., Fernández-López, D., Díaz-Guzmán, J., Negredo, P., Avendaño, C., Castellanos, M., Gasull, T., Dávalos, A., Moro, M.A., Lizasoain, I., 2018. Iron overload exacerbates the risk of hemorrhagic transformation after tpa (tissue-type plasminogen activator) administration in thromboembolic stroke mice. Stroke 49 (9), 2163–2172.

Millan, Mónica, Sobrino, Tomás, Castellanos, M., Nombela, F., Arenillas, J.F., Riva, E., Cristobo, Iván, García, M.M., Vivancos, José, Serena, Joaquín, Moro, M.A., Castillo, José, Dávalos, A., 2007. Increased body iron stores are associated with poor outcome after thrombolytic treatment in acute stroke. Stroke 38 (1), 90–95.

Hanafy, K.A., Gomes, J.A., Selim, M., 2019. Rationale and current evidence for testing iron chelators for treating stroke. Curr. Cardiol. Rep. 21, 20. https://doi.org/10.1007/s11886-019-1106-z.

Kosyakovsky, J., Fine, J.M., Frey 2nd, W.H., Hanson, L.R., 2021. Mechanisms of intranasal deferoxamine in neurodegenerative and neurovascular disease. Pharmaceuticals (Basel, Switzerland). 14, 95. https://doi.org/10.3390/ph14020095.